A&A 545, L3 (2012)
DOI: 10.1051/0004-6361/201219538

Astronomy & Astrophysics

Letter to the Editor

Discovery of an X-ray cavity near the radio lobes of Cygnus A indicating previous AGN activity

Gayoung Chon[1], Hans Böhringer[1], Martin Krause[2,1], and Joachim Trümper[1]

[1] Max-Planck-Institut für extraterrestrische Physik, 85748 Garching, Germany
e-mail: gchon@mpe.mpg.de
[2] Excellence Cluster Universe, Technische Universität München, Boltzmannstrasse 2, 85748 Garching, Germany

Received 4 May 2012 / Accepted 8 August 2012

ABSTRACT

Cygnus A harbours the nearest powerful radio jet of a Fanaroff-Riley (FR) class II radio galaxy in a galaxy cluster where the interaction of the jet with the intracluster medium (ICM) can be studied in detail. We use a large set of *Chandra* archival data, VLA, and other new radio observations to shed new light on the interaction of the jets with the ICM. We identify an X-ray cavity in the distribution of the X-ray emitting plasma in the region south of the Cyg A nucleus, which has lower pressure than the surrounding medium. The radio observations show that the cavity is filled with synchrotron emitting plasma. The spectral age and the buoyancy time of the cavity indicates an age that is at least as old as the current Cyg A jets and not much older than twice this time. We suggest that this cavity was created in a previous active phase of Cyg A when the energy output of the active galactic nucleus was about two orders of magnitude less than today.

Key words. X-rays: galaxies: clusters – galaxies: clusters: intracluster medium – radio continuum: galaxies – galaxies: jets

1. Introduction

Active galactic nucleus (AGN) feedback in galaxy clusters has gained a lot of attention in recent studies, e.g. McNamara & Nulsen (2007). Most of the AGN in clusters are FR I radio sources. In the local Universe, Cygnus A is an exception featuring a powerful FR II radio jet in a galaxy cluster where very energetic interaction effects of the jets with the intracluster medium (ICM) can be studied in detail: e.g. Carilli & Barthel (1996), Clarke et al. (1997), Kaiser & Alexander (1999), and Krause (2005). In this object we can observe jets of relativistic synchrotron emitting plasma ploughing into the ICM out to a distance of ∼100 kpc from the nucleus where they end in hotspots clearly seen at radio wavelengths (e.g. Alexander et al. 1984) and X-ray images (e.g. Harris et al. 1994). The internally supersonic jet plasma is thermalised at these hotspots, which advance only at about 2000 km s^{-1} owing to the extreme density contrast (Alexander & Pooley 1996). The jet plasma flows away from the overpressured hotspots, thereby establishing a backflow. Together with the adjacent ICM, this region defines an overpressured bubble that drives a shock into the undisturbed ICM, first seen by Carilli et al. (1988) in the centre of the Cyg A cluster.

Many aspects of Cyg A have been studied in both radio and X-rays: e.g. Carilli et al. (1994), Wilson et al. (2000, 2006), Smith et al. (2002), and Yaji et al. (2010). Some progress has been made recently in modelling these jets with hydrodynamical simulations (Krause 2003, 2005; see also Alexander & Pooley 1996). The observed width of the radio lobes are only reproduced by very light jets, with jet densities of the order of 10^{-4} times the already tenuous surrounding X-ray plasma. This implies a low momentum flux and low hotspot advance speeds, comparable to the general advance speed of the bow shock driven into the surrounding ICM. Consequently, the bow shock assumes an almost spherical shape around the radio source with a wide region of shocked ICM adjacent to the radio lobes.

In this paper we use most of the *Chandra* archival data on Cyg A to study the interaction effects in the region near the AGN inside the radio lobes in detail. In this region we have discovered an X-ray cavity very similar to those found in FR I radio sources in clusters. We investigated it in detail with the X-ray and radio data to unveil its physical properties and its origin, and interpreted them with a hydrodynamical simulation.

For distance related quantities we adopt a flat Λ-cosmology with $H_0 = 70$ km s^{-1} Mpc^{-1}, $\Omega_M = 0.3$. For the redshift of Cyg A of 0.0561, 1″ corresponds to 1.09 kpc.

2. *Chandra* observations

We used all available archival *Chandra* ACIS-I observations for Cyg A, which sum up to 200 ks of exposure. Standard data analysis was performed with CIAO 4.4[1] with calibration database (CALDB) 4.4.8. This includes flare cleaning by filtering light curves of source-free regions, VFAINT mode, gain, and charge transfer inefficiency corrections. The final exposure after cleaning is slightly less than 190 ks. We apply the same procedure to an ACIS blank sky observation, which was used as our background estimate after adjusting the normalisation. In our case different normalisations of the background do not significantly influence the results of our analysis since the region of our interest has high source counts. We used the 9−12.5 keV count-rate to get the appropriate normalisation for the background exposure. We used *fluximage* to obtain flux and exposure maps after background subtraction, and the combined map is shown

[1] http://cxc.harvard.edu/ciao4.4/index.html

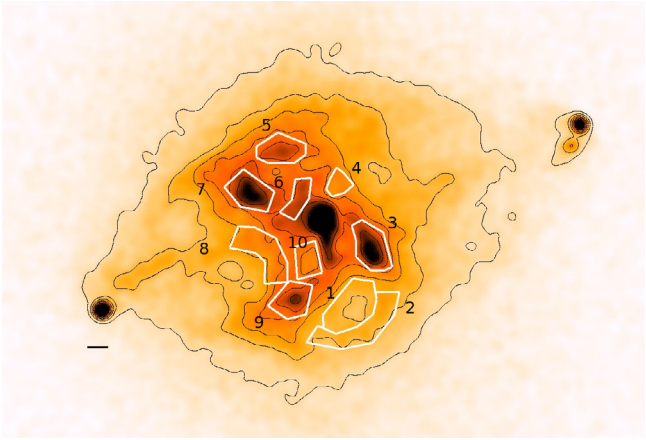

Fig. 1. *Chandra* image of Cygnus A with contours and ten study regions in white polygons with their ID numbers. The dimension of the image is 2.6′ × 1.75′, and a black line of length 5″ is marked below the eastern hotspot. The X-ray cavity, 1, is the polygon defining a region of low X-ray surface brightness.

in Figs. 1 and 3 in the 0.5−2 keV band. Figure 1 shows a detailed image of Cyg A with X-ray contours in an area of 2.6′ × 1.75′. There are ten regions defined by white polygons with their ID numbers, for which we determine the X-ray properties in the next section.

3. Properties of the X-ray cavity

Figure 1 shows the detailed X-ray surface brightness distribution in the shocked region of Cyg A. The shocked region is contained in an ellipse surrounding two hotspots and the jets and extends outside the outermost contour in Fig. 1. From radio observations we know that the energetic jet created backflows, which are seen as diffuse lower surface brightness areas starting near the hotspots towards the centre. The central region away from the heads of the jets and backflows is expected to be in pressure equilibrium. An interesting region drawing attention is the low surface brightness feature numbered 1. This is the "cavity" we study in this paper with a lower-than-expected thermal plasma pressure.

The goal of the X-ray analysis is then to extract first spectra for determining temperatures, calculating electron densities, n_e, and then pressures to characterise the cavity and its vicinity to diagnose the pressure distribution. The value of n_e is derived from the X-ray luminosity, $L_X = \int dV n_e^2 \Lambda(T)$, and temperatures are determined by fitting the observed spectrum in XSPEC with an absorbed MEKAL model.

We defined ten regions of roughly homogeneous surface brightness and sufficient source counts in the centre of Cyg A around region 1. For comparison four regions (3, 5, 7, 9) were similarly defined as in Smith et al. (2002), and Wilson et al. (2006). Our fitted temperatures from these four regions agree well with theirs within our uncertainties. We find the temperature in region 1 to be 5.35 ± 0.31 keV with a metallicity 0.81 ± 0.12 $Z_\odot$ and a column density of 0.3 ± 0.02 × 10^{21} cm^{-2}. The temperatures and pressures from all regions are listed in Table 1 where the region numbering follows Fig. 1. The fitting results for the temperature are stable against variations in the metal abundances and the initial values of the fit parameters thanks to the exceptionally good photon statistics.

To calculate the pressure inside each region, a geometry of the volume needs to be assumed, which in principle introduces the largest uncertainty for this work. We assume the shocked region is contained in a cylinder with an axis connecting the two hotspots and a radius of 100 kpc. This radius is chosen since simulations show the shock radius along the semi-minor axis to be roughly 100 kpc (Krause 2005). The length of each region is then the distance it extends along the line of sight contained in the cylinder. With this definition we calculated the density and the thermal pressure of the ten regions listed in Table 1. We expect all ten regions to be in near thermal pressure equilibrium. However, our findings show that the region 1 contains the smallest contribution from the thermal pressure among the ten areas. In Fig. 2 the measured temperature and derived n_e are compared with the average pressure equilibrium.

The statistical error of n_e is very small, while the systematic error is dominated by the assumption on the geometry of the volume associated with the various selected study regions in the sky. If for example the radius of the cylinder is different by a factor of 1.4 compared to our assumption, this translates into an 18% uncertainty of the density. For the comparison in Fig. 2 we are interested in the uncertainties of the differences between the regions. For the relative uncertainties between regions with different distances from the centre we find values up to 9%. We expect that other viable variations in the geometry will not

Table 1. X-ray temperatures and pressures of the ten regions defined in Fig. 1.

Regions	T (keV)	ΔT (keV)	P (10^{-10} erg/cm^3)
1 (Cavity)	5.35	0.31	3.77
2	5.58	0.33	4.40
3	3.74	0.12	4.06
4	5.75	0.55	4.87
5	4.04	0.16	4.51
6	3.77	0.18	4.00
7	4.17	0.15	5.02
8	5.73	0.28	5.04
9	4.07	0.17	4.50
10	5.06	0.36	4.56

Notes. The largest uncertainties in the pressure are contributed by the estimated length of the region along the line of sight. For details see text.

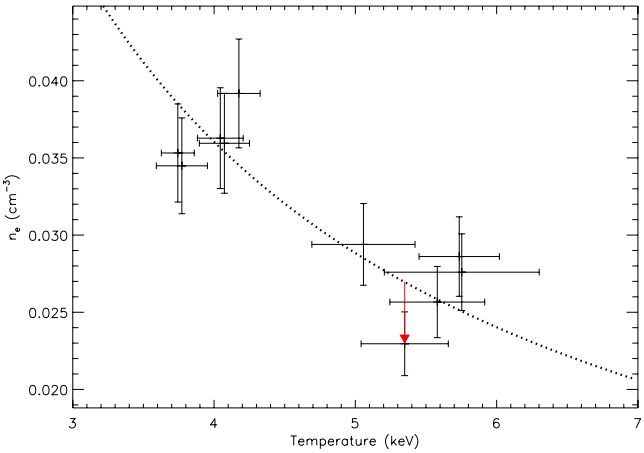

Fig. 2. Electron density against temperature of the ten regions around the X-ray cavity. We expect to have an equi-pressure in the central ICM, which is indicated by a dashed line. The largest departure from the expected pressure is exhibited by the cavity of our study marked by a red arrow. We used a highly conservative systematic error for the electron density, n_e (see texts for the assumptions).

yield larger uncertainties. Therefore we have conservatively used these systematic uncertainties for the error bars in Fig. 2. The cavity region thus shows a deviation from the expectation value about a factor of 2.7 higher than our upper uncertainty limit.

The pressure deficit can be interpreted as a 30% smaller volume or a 16% deficit in the density. Here we continue with the hypothesis that the missing thermal pressure in the volume can be explained by introducing non-thermal pressure support. In the next section we use this 30% deficit of the volume to calculate the relativistic plasma and magnetic field properties.

4. Properties of the relativistic plasma in the cavity

Using radio observations we now search for an explanation of the missing cavity pressure through a relativistic plasma, which could make up for this deficit. We compared X-ray images of Cyg A with radio maps from Very Large Array (VLA) and LOFAR observations. Two VLA observations are at 74 and 327 MHz from Lazio et al. (2006), and the new commissioning LOFAR data at 238 MHz is from McKean et al. (2011). The overlay with the 327 MHz VLA observation is shown in the upper panel of Fig. 3. It is obvious that the X-ray cavity coincides perfectly with the radio emission region extending out from the bridge between the radio lobes south of the nucleus. The highest contours trace the cavity region well while the lowest contours also encompass the cavity rim.

As argued in the previous section, the missing thermal pressure can be partly explained if 30% of the cavity volume is filled with relativistic plasma. We imagine this cavity volume to be contiguous and completely occupied by relativistic plasma alone. We could, however, also have another scenario, where the cavity is filled by both plasmas characterised by two partial filling factors. In this case the cavity volume has to be larger by the inverse of the filling factor of the relativistic plasma, so that the effective volume occupied by the non-thermal plasma stays the same. In this case all the following calculations and considerations stay the same, as for the case of the cavity devoid of thermal plasma. If both plasmas are completely mixed in the cavity volume, the calculations of the pressure contributions of the two phases are still similar to the non-unity filling factor case and the volume of the cavity has to be similarly enlarged to fulfil the observational boundary conditions. Therefore in this section we calculate the relativistic plasma and magnetic pressure for the cavity devoid of thermal plasma, keeping in mind that this solution can be easily scaled to the other two scenarios with unchanged conclusions.

Radio observations provide information on the energy loss of the relativistic electrons in a magnetic field through synchrotron radiation. The magnetic field strength is conventionally derived by minimising the total energy content in the volume based on the equipartition argument. The magnetic field energy is proportional to the square of the magnetic field strength, while the total electron energy is calculated by integrating the product of its density and energy distribution. The total plasma energy of a volume can then be written in terms of the magnetic field strength, $E_{\rm tot} \propto \alpha(1+k)LB^{-3/2} + B^2\Phi V/8\pi$ where k is the ratio of proton to electron energy, L the intensity of the radio emission, Φ the filling factor describing the fractional volume that the magnetic field occupies, and V the volume of interest (e.g. McNamara & Nulsen 2007). The corresponding pressure of the total energy in relativistic plasma plus magnetic field is then $13/9\ B^2/8\pi$ (Pacholczyk 1970).

The radio flux density and spectral index were determined based on the multi-frequency data mentioned earlier. The flux densities of the cavity are estimated to be 234 and 35 Jansky at 74 and 327 MHz for VLA observations. We do not give the flux density determined with the LOFAR data on request by the LOFAR collaboration in this paper; however, we note that the spectral index determined including the LOFAR flux density is consistent with what is determined by the VLA data alone. The spectral index between the two extreme bands is then 1.2, and 1.24 between 74 and 238 MHz. Conservatively allowing an error of 50% on the 74 MHz observation, we find a spectral index between 1.0 and 1.5. Thus we adopt 1.24 for further calculations, but we checked that the conclusions do not change if the spectral index is varied within these limits. It was noted that the spectral index of the lobes around the hotspots is around 0.5 (Lazio et al. 2006), and we expect the cavity spectral index to be much steeper than 0.5 containing an older electron population.

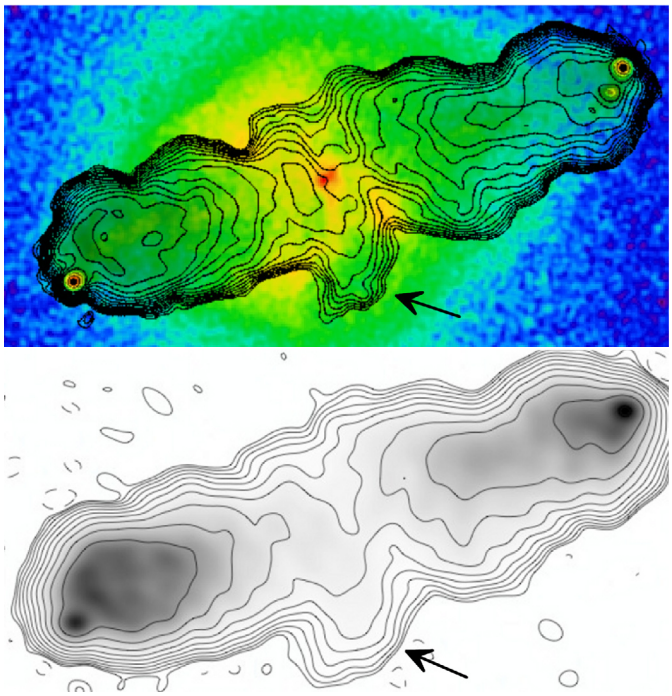

Fig. 3. *Upper panel*: overlay of a VLA radio map at 327 MHz as contours on the *Chandra* image. The VLA contours are taken from Fig. 2 of Lazio et al. (2006). The low surface brightness cavity of our study in the X-ray image spatially matches the excess in the radio contours. The cavity is enclosed by a brighter rim in the south. *Lower panel*: the LOFAR contours are taken from Fig. 1 of McKean et al. (2011). On request by the LOFAR collaboration we do not show an overlay with the LOFAR data. However, we emphasise that the location of our X-ray cavity coincides exactly with the radio excess shown by the LOFAR contours as well. To guide the eye both figures are on the same scale. In both panels the location of the X-ray cavity is indicated by an arrow.

Using the mentioned equipartition argument, we calculated the plasma properties for given flux density, spectral index, filling factor unity, and a lower integral limit of the synchrotron luminosity of 1 GeV. This is reasonable given the characteristic electron energy at 74 MHz with a magnetic field of 17 μG is 8.9 GeV. We find 1.18×10^{-11} erg/cm^3 for the magnetic field energy density, 1.58×10^{-11} dyne/cm^2 for the total relativistic plasma pressure, and a magnetic field of 17.2 μG. The total non-thermal pressure we calculated falls short to make up for the missing thermal pressure in the previous section. However, we stress that what we calculated is the *minimum* pressure. Uncertainties could modify our scenario; for example, a higher proton energy ratio such as $k = 100$, would increase the

non-thermal pressure up to 46% of the thermal pressure compared to 7% as in our case. Other open factors that influence the results are the geometry of the volume element, as mentioned earlier, and the lower integral limit for the total electron energy.

From these physical parameters and some further observables we can also derive information on the age of the cavity. One constraint is derived from the cavity filled with relativistic plasma having much lighter than the ambient medium, and we thus expect it to be buoyantly rising in the cluster potential (Churazov et al. 2000). Assuming the buoyant velocity can be calculated from $v_b = 0.5\sqrt{r/R}v_k$ where v_k is the Kepler velocity, we obtain a buoyant rise time of 50 Myr for the present distance, $R = 23$ kpc, of the bubble from the centre. We interpret this as an approximate upper limit of the bubble age, as we would expect an older bubble to have moved to a larger radius. Here the cluster was modelled with an isothermal β profile (Smith et al. 2002) with core radius 29″ and $\beta = 0.67$, and assuming the cavity volume contains negligible thermal plasma.

We can estimate the minimum age for this cavity assuming that electrons lose most of their energy through synchrotron radiation in the magnetic field. If we adopt the break frequency at 750 MHz determined by Carilli et al. (1991) and our results for the magnetic field strength in the cavity, we obtain a spectral age of 24 Myr. It is interesting that the spectral age map in Fig. 8 of Carilli et al. (1991) shows the X-ray cavity region as the oldest electron population in the core of Cyg A. This fits with our suggestion below that the X-ray cavity was created earlier than the current jets, possibly by a less energetic feedback event.

5. Discussion

We can now compare the estimated age of the X-ray cavity to the age of the jet and the radio lobes of Cyg A. The time duration of the present high power activity and the age of the radio lobes estimated from simulations and observations is about 30 Myr (Krause 2005; Wilson et al. 2006). This is close to the estimated cavity age within a factor of a few, but the limits we derived above also allow the cavity to easily be older by a factor of two. This provides some constraining information for the search of the origin of the cavity. One possible explanation is that the cavity is part of the backflow of the relativistic plasma from the hotspot region. It might have been broken off from the main lobes by an instability or as proposed in Carilli et al. (1991) by deflection of the backflow. In this case the cavity and the lobes would be expected to be of similar ages. However, dynamically this is not easily possible since the growth timescale of e.g. Rayleigh-Taylor instabilities is ≥50 Myr, which is much larger than the age of the current radio source.

We offer, however, another explanation, where the radio plasma in the cavity has been created in a previous phase of jet activity at a lower power output. We envision a scenario where the effect of the jets is similar to those in the Perseus cluster, where two radio bubbles were inflated close to the nucleus, creating cavities in the X-ray emitting gas (Böhringer et al. 1993; Fabian et al. 2002). If the jets have had a more north-south direction, and if the radio bubbles have partly been pushed off and partly started to rise due to buoyancy, we would expect to observe a cavity towards the south like the one we see.

The enthalpy necessary to create the cavity can be used as an estimate of the AGN jet energy output in this past event. Assuming the enthalpy is given by $4PV$ (with P the pressure, V the volume of the cavity), we find an energy output of the AGN of the order of 2.2×10^{59} erg. For an activity duration of about 5−30 Myr, the AGN power output in form of mechanical energy amounts to $\sim 2-14 \times 10^{44}$ erg s^{-1}. This is about two orders of magnitude below the current AGN power, well in line with the scenario where the jets have gently inflated bubbles close to the AGN rather than creating powerful jets that plough far out into the cluster ICM like at the present time.

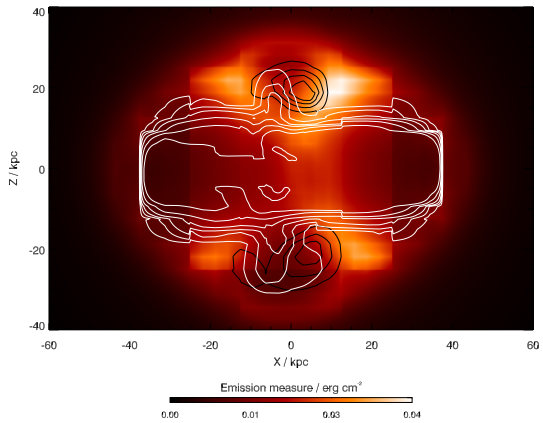

Fig. 4. Simulated X-ray emission measure map of the interaction of two perpendicular jets in Cyg A. The four bright regions are shaped by the cavities of the first jets. The cavities of the main jets are also visible. Black contours show the volume fraction of the first jets at $2^n \times 10^{-5}$. That of the main jets is at 1, 3, 6, 12, 24, and 48 $\times 10^{-3}$ in white. Rectangular features are due to artifacts of the nested static grid setup.

We have further investigated this hypothesis with 3D-hydrodynamics simulations with the NIRVANA code (Ziegler 2008). With a static gravitational potential, two jets are injected by adding energy, momentum, and mass to a cylindrical region with a radius of 0.2 kpc. First, a low power jet (10^{45} erg s^{-1}) is injected along the Z-axis for 5 Myr. After a 5 Myr break, the main jet (2×10^{47} erg s^{-1}) is started and evolved for 7.8 Myr. We show the resulting emission measure map along with contours of the two jet tracers through the midplane in Fig. 4. Interestingly, the X-ray cavities created by the first jets are preserved during the expansion of the main jet, and just pushed outwards. A characteristic feature of this model are the four bright regions, which appear owing to the presence of the old cavities separating them in the middle. This bears a striking resemblance to the X-ray observation of Cyg A. The jet tracers show that the plasma of the first jet was pushed towards the edges. Lobe plasma from the second jet and some thermal plasma have filled the cavity, and the second jet plasma dominates the cavity pressure. The amount of the latter might in reality be somewhat suppressed due to the stabilising effect of magnetic fields. If in fact new plasma refills the old cavity, some of our above conclusions may be modified. At the simulation time of 7.8 Myr after launch of the main jets, they have not yet expanded to the presently observed size. The effects discussed here are, however, clearly demonstrated, which include the approximate size of the cavity. Since the simulation employed 1.6×10^{59} erg for the first jet pair, this confirms our order-of-magnitude estimate of the energy of the previous event.

6. Conclusions

We have combined most of the available *Chandra* X-ray data to construct a very detailed image of the ICM in the central region of Cyg A. The region around the AGN is rich in structure, and one of the most striking features is an X-ray cavity south of the nucleus, which is reminiscent of similar cavities in other cool cores of galaxy clusters. A comparison of the X-ray image with radio maps from VLA and LOFAR observations shows

that the cavity is filled with relativistic plasma with a total enthalpy of 2.2×10^{59} erg. The most natural explanation in our opinion of the radio plasma filled cavity is an origin from previous activity of the AGN before the present radio lobes and shocked ICM region were created, more than about 30 Myr ago. The appearance of the cavity and the X-ray morphology in the centre of Cyg A is reproduced well by our simulation of this scenario. In this case the power of the jets at this earlier epoch was about 100 times lower than today, also consistent with the simulation results. Thus Cygnus A would have been classified at this epoch as an FR I radio source. If our interpretation is correct we have the first evidence that an FR II radio source today was an FR I source at an earlier time.

Acknowledgements. We thank the referee for the comments, and Paul Nulsen for interesting discussions. M.K. and H.B. acknowledge support by the cluster of excellence "Origin and Structure of the Universe" (`www.universe-cluster.de`). H.B. and G.C. acknowledge support from the DfG Transregio Program TR 33. G.C. acknowledges support from Deutsches Zentrum für Luft und Raumfahrt(DLR). This research has made crucial use of VLA and *Chandra* data and of software provided by the Chandra X-ray Center (CXC), and NIRVANA code v3.5 developed by Udo Ziegler at the Leibniz-Institut für Astrophysik Potsdam.

References

Alexander, P., & Pooley, G. G. 1996, Cygnus A – Study of a Radio Galaxy (Cambridge University Press)
Alexander, P., Brown, M. T., & Scott, P. F. 1984, MNRAS, 209, 851
Böhringer, H., Voges, W., Fabian, A. C., et al. 1993, MNRAS, 264, 25
Carilli, C. L., & Barthel, P. D. 1996, A&ARv, 7, 1
Carilli, C. L., Perley, R. A., & Dreher, J. W. 1988, ApJ, 334, L73
Carilli, C. L., Perley, R. A., Dreher, W. W., & Leahy, J. P. 1991, ApJ, 383, 554
Carilli, C. L., Perley, R. A., & Harris, D. E. 1994, MNRAS, 270, 173
Churazov, E., Forman, W., Jones, C., & Böhringer, H. 2000, A&A, 356, 788
Clarke, D. A., Harris, D. E., & Carilli, C. L. 1997, MNRAS, 284, 981
Fabian, A. C., Sanders, J. S., Crawford, C. S., et al. 2002, MNRAS, 331, 369
Harris, D. E., Carilli, C. L., & Perley, R. A. 1994, Nature, 367, 713
Kaiser, C. R., & Alexander, P. 1999, MNRAS, 305, 707
Krause, M. 2003, A&A, 398, 113
Krause, M. 2005, A&A, 431, 45
Lazio, T. J. W., Cohen, A. S., Kassim, N. E., et al. 2006, ApJ, 642, L33
McKean, J., Ker, L., van Weeren, R. J., et al. 2011 [`arXiv:1106.1041`]
McNamara, B., & Nulsen, P. 2007, ARA&A, 45, 117
Pacholczyk, A. G. 1970, Radio Astrophysics (Freeman)
Smith, D. A., Wilson, A. S., Arnaud, K. A., et al. 2002, ApJ, 565, 195
Wilson, A. S., Young, A. J., & Shopbell, P. L. 2000, ApJ, 544, L27
Wilson, A. S., Smith, D. A., & Young, A. J. 2006, ApJ, 644, L9
Yaji, Y., Tashiro, M., Isobe, N., et al. 2010, ApJ, 714, 37
Ziegler, U. 2008, Comput. Phys. Commun., 179, 227